scientific reports

Check for updates

OPEN

# Knot formation of dsDNA pushed inside a nanochannel

Jan Rothörl[1], Sarah Wettermann[1], Peter Virnau[1]✉ & Aniket Bhattacharya[2]✉

**Recent experiments demonstrated that knots in single molecule dsDNA can be formed by compression in a nanochannel. In this manuscript, we further elucidate the underlying molecular mechanisms by carrying out a compression experiment in silico, where an equilibrated coarse-grained double-stranded DNA confined in a square channel is pushed by a piston. The probability of forming knots is a non-monotonic function of the persistence length and can be enhanced significantly by increasing the piston speed. Under compression knots are abundant and delocalized due to a backfolding mechanism from which chain-spanning loops emerge, while knots are less frequent and only weakly localized in equilibrium. Our in silico study thus provides insights into the formation, origin and control of DNA knots in nanopores.**

In many biological processes a double-stranded DNA (dsDNA) is confined in a geometry much shorter than its contour length in a highly organized and compact state and often under high pressure[1,2]. A classic example is an organized state of a dsDNA strand in a viral capsid[3–8]. The viral DNA uses the stored elastic energy for its invasion process. Intriguingly, this DNA was found to be highly knotted particularly in a mutant variant for which both sticky ends are allowed to reside within the capsid[3,4]. It is in general difficult to develop an experimental protocol to study an actual system in vitro, although there have been studies to measure the force and the organized topology of the dsDNA inside a capsid[9,10]. During the last decade advancements in nanotechnology have enabled us to prepare nanochannels of sub-persistence length dimensions[11]. DNA pushed inside nanofluidic devices[12–16] is now used for mapping genomes, sequence motifs, structural variations[17,18].

Recently, nanochannels were even used for the detection of knots in DNA as demonstrated in experiment[19] and simulation[20]. Due to a controllable and simpler geometry, nanochannels offer immense promise to understand universal aspects of biological phenomena using well established concepts from polymer physics[21,22]. Besides problems of biological significance and of human health, nanochannel based experiments claimed the occurrence of jamming[9,10]- which indicates that confined bio-polymers offer yet another platform to study slow relaxation and glassy dynamics. Thus studies of chain compression in nanochannels appeal to broad areas of science.

Many numerical studies of knots have established numerous results on generic[23–38] and biopolymers[1,6,8,39–45]. While knots are, e.g., abundant in single ideal chains[24,25], the addition of excluded volume typically reduces the knotting probability significantly[25,29], while spherical confinement or globular states enhance knotting[26,29]. For the latter, knots tend to be delocalized, i.e. average sizes scale linearly with the chain length[29], while knots are weakly localized and scale sub-linearly for under ideal or good solvent conditions[28,29].

Previously, we have studied compression of semi-flexible polymers in nanochannels using a Langevin dynamics (LD) scheme[46,47]. These LD simulation studies and another recent study[48] have provided substantial insights about many details at smaller length scales unattainable experimentally, but are essential for microscopic understanding and interpretation of nanochannel experiments using fundamental laws of physics. One of the advantages of these simulation studies is that, unlike an actual experiment, one can vary confining dimensions and chain stiffness easily and is thus capable of extending the simulation studies for a broader parameter space which is often quite expensive to design experimentally. In our recent LD simulation study[47] we mimicked a recent experiment in silico where dsDNA—modeled as a semi-flexible polymer—was pushed inside a rectangular open-ended nanochannel much longer than required to attain a steady state. By varying the bending rigidity of the chain we showed how the structure evolves from a disordered state to a highly organized spooled state. Furthermore, the LD simulation revealed a detailed picture of how the fold nucleation originates at the piston end and expands during the compression process[47].

An important and relevant question in these compression studies in the biological context is to study how the formation of knots are initiated and once formed how they spatially evolve under confinement. Theoretical and

[1]Institut für Physik, Johannes Gutenberg-Universität, Staudinger Weg 9, 55099 Mainz, Germany. [2]Department of Physics, University of Central Florida, Orlando, FL 32816-2385, USA. ✉email: virnau@uni-mainz.de; Aniket.Bhattacharya@ucf.edu

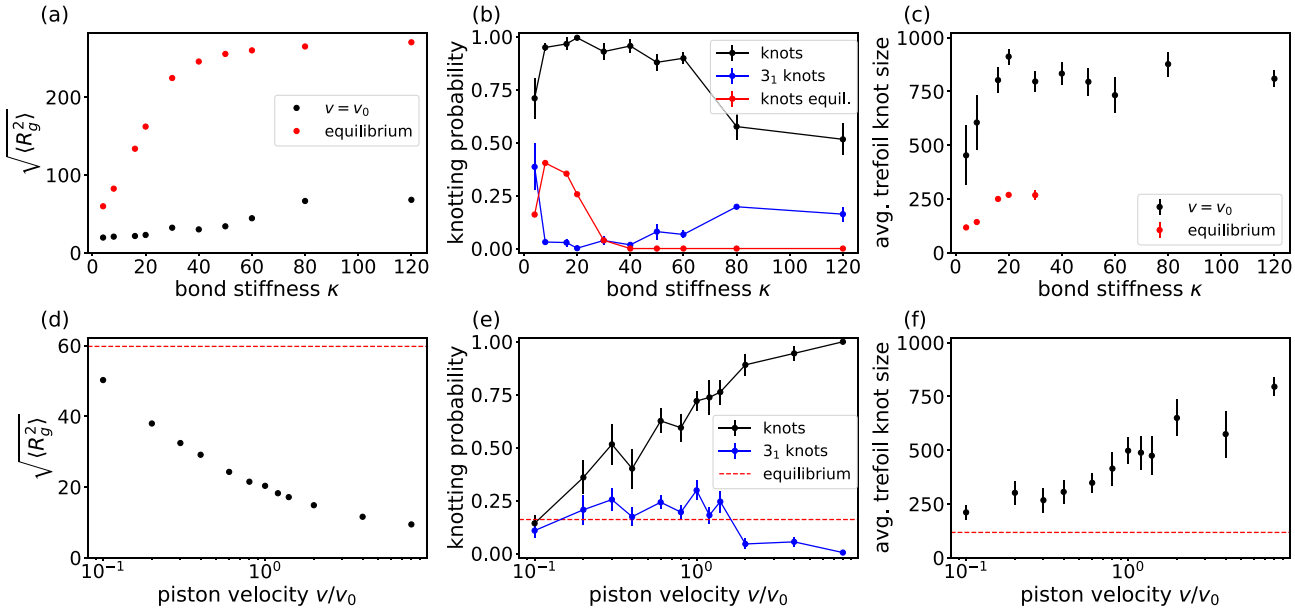


**Figure 1.** Knots and radii of gyration of steady-state configurations for different input parameters. (**a**) Root-mean-squared radius of gyration $\sqrt{\langle R_g^2(t)\rangle}$ for chains of different stiffness. Error bars are omitted as their size is smaller than the size of the points. (**b**) Knotting probability and occurrence probability of trefoil knots for different values of the bond stiffness $\kappa$. Error bars are determined by taking the standard deviation over the square-root of the number of runs. Lines are added for readability. Knotting probability for $v = 0$ is strictly zero for $\kappa \geq 50$. (**c**) Trefoil knot lengths found for different $\kappa$ with a moving piston and in equilibrium. (**d**) $\sqrt{\langle R_g^2(t)\rangle}$ for different piston velocities at $\kappa = 4$. Again the size of error bars would be smaller than the size of the points. The red dashes in (**d**–**f**) indicate the average result in MC simulations without a moving piston for $\kappa = 4$ which is equivalent to the leftmost equilibrium values in plots (**a**–**c**). (**e**) Knotting probabilities for different piston velocities at $\kappa = 4$. (**f**) Trefoil knot lengths for different piston velocities at $\kappa = 4$.

simulation studies have been further fueled by a recent experiment that demonstrates that knots indeed occur in compression experiments[16]. In computer simulations studies Orlandini and Micheletti have already investigated equilibrium knot formation of coarse-grained DNA models in nanonchannels[31,32]. Of particular relevance to our work is a recent study[38] in which the non-equilibrium formation of knots and so-called geometrical entanglements as measured by counting crossings under projections are investigated in closed nanochannels exposed to compression and relaxation cycles. It was found that the two types of entanglements evolve with different dynamics and are for the most part uncoupled.

Here, we investigate knot formation when a confined dsDNA is being pushed by a nano-dozer in a nanochannel whose width is much smaller than the contour length of the dsDNA. An important difference from previous studies is that our system is open ended in one direction and that we study the evolution of knots in a constantly moving steady state. We also vary the bond stiffnesses to investigate the influence of changes in salt conditions. The key result is that the confined chain in the nanochannel pushed by a nano-dozer will progressively become highly knotted with delocalized knots. The knotting probability is greatly enhanced compared to corresponding equilibrium simulations, which in addition to compactification can be traced back to a backfolding mechanism for semi-flexible chains. Next, we describe the model, some essential facts about the LD simulation scheme, how our coarse-grained chains can be mapped onto DNA and the method that we use to analyze knots.

## Results

**Emergence of knots in nanochannels.** Figure 1 summarizes the main findings of our study. Applying a pushing force leads to a compactification of the polymers (Fig. 1a), which in turn dramatically increases the occurrence of knots in the steady state in comparison to equilibrium values (Fig. 1b). Likewise, the amount of trefoil knots is reduced for configurations with a higher total knotting probability because the high density induces the formation of multiple or more complex knots. In this compact state, knots are delocalized and span over the whole chain as indicated for the example of trefoil knots in Fig. 1c where for a bending stiffness $\kappa > 20$ the average length of the knot is approximately 80% of the contour length or higher, which implicates that knots are formed preferentially near each end (please see Fig. 2e), while knots in equilibrium conformations are significantly smaller. These findings in a sense mirror previous observations, e.g. in Ref.[29], which demonstrated that a $\theta$-transition from a swollen coil to a globular state is not only accompanied by an increase in knotting but also by a delocalization of the latter.

Figure 1d investigates the influence of the piston velocity for the experimentally relevant case of $\kappa = 4$ (DNA in a nanochannel, see "Methods" section). Again, compactification with increasing velocity is directly related to an increase of overall knotting. These results suggest that the occurrences of knots can be tuned by the speed

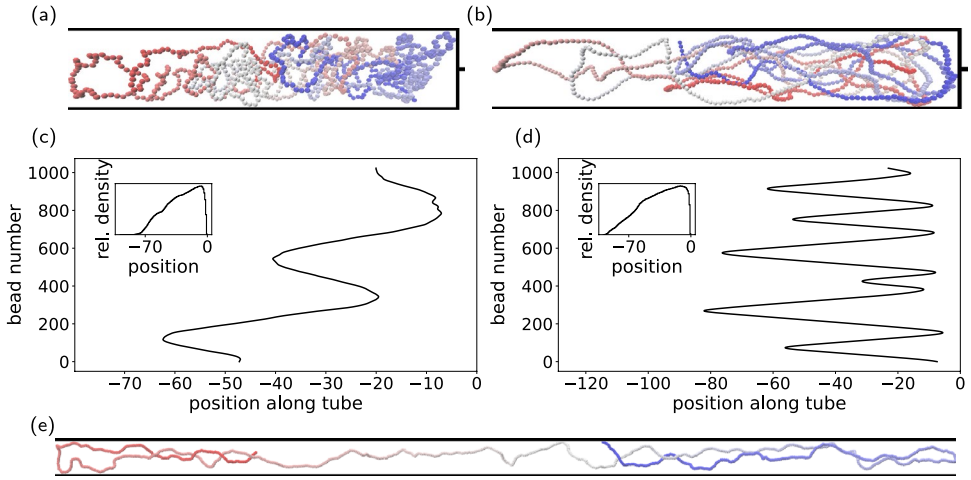


**Figure 2.** Simulated structures for different parameters. (**a**, **b**) Structures for $\kappa = 4$ (**a**) (length parallel to the channel $73\sigma$) and $\kappa = 20$ (**b**) (length $91\sigma$) visualized using VMD[49]. Beads are colored from blue to red according to their monomer number. (**c**, **d**) The plots show the average position along the tube for all beads averaged over a simulation time of $50,000\tau$ for simulations at $\kappa = 4$ (**c**) and $\kappa = 20$ (**d**) with the piston at position 0. The insets show the relative density of beads along the structure averaged over the same frames. The structure for $\kappa = 20$ is significantly larger. The highest density for both structures is found to be close to the piston on the right. (**e**) Equilibrium structure without piston for $\kappa = 20$.

of the piston and converge towards the equilibrium values for small piston velocities (Fig. 1e). This outcome is similar to results of Michieletto et al.[38] indicating that an increased piston force will lead to an increase in the overall knotting probability and knot complexity as shown by a decrease in the occurrence of simple trefoil knots. As indicated above the decrease of knotting towards the equilibrium state at slow piston velocities is again accompanied by a trend towards a weak localization of trefoil knots (Fig. 1f)[29].

Figure 2 sheds light on these findings from a molecular basis. For $\kappa = 4$ the structure is disordered but the position of the monomers is still correlated with their sequence as indicated by the color scheme in Fig. 2a and the bead positions in Fig. 2c. For $\kappa = 20$, the persistence length already exceeds the width of the tube which in conjunction with compactification leads to backfolding (Fig. 2b,d). The backfolding on the other hand creates loops which are a prerequisite for knots and in turn explains the initial rise in knotting with $\kappa$ as well as their delocalization. In this context it would be interesting to study if backfolding creates a prevalence of torus-type knots as e.g. observed in the DNA located in viral capsids[4,7]. Unfortunately, the statistics of our simulations do not allow for a meaningful comparison. For large persistence lengths, backfolding becomes more difficult resulting in a lower knotting probability (Fig. 1b). In the equilibrium case, the compactification from the piston is no longer present and for $\kappa = 20$, the chain can already spread throughout the channel which leads to a low knotting probability and weakly localized knots (Fig. 2e).

## Discussion

In this manuscript we investigate velocity induced knot "production" in a nanochannel in comparison to those under equilibrium conformations. Both knotting probability and knot sizes depend strongly on piston velocity and resulting compactification as well as chain stiffness which can be, e.g., mitigated by adjusting ionic conditions and screening of charges in DNA. We observe that if the chain's persistence length is greater than the width of the nanochannel, knots form by a backfolding mechanism. Since backfolding becomes harder for larger stiffness, the probability of knot formation decreases which explains the observed non-monotonic characteristic of knot formation in a nanochannel. We also study relative occurrences of complex knots as a function of the piston velocity and the chain stiffness. Our study thus sheds some new light on recent experiments in which DNA knots were created in a flow channel[16] and provides insight on the molecular origin and control of self-entanglements under these conditions.

Finally, we would like to point out that the coarse-grained simulation does not include hydrodynamic effects. It is worth considering how the results will change if we had incorporated it in the simulation. Dorfman has argued that for flexible chains hydrodynamic interactions are important. But for the semi-flexible chains with persistence length larger than the pore width, the chain is fully extended and is described by the free-draining limit[50]. Thus, for most channel sizes which result in a significant extension of the DNA compared to its bulk conformation, the hydrodynamic interactions between segments of the chain are almost completely screened. For the parameters used here the chain conformation lies in the transition region between deGennes blobs and Odjik limit and there is no theoretical argument for the effects of the hydrodynamic interaction in this regime. However, from Fig. 2 we observe that the chain conformations are mostly extended and hydrodynamic effects are likely to be small. For large velocities folded conformations are very different from deGennes blobs and therefore, one would expect the hydrodynamic effects to be small also, and the conclusions of this manuscript will essentially remain the same.

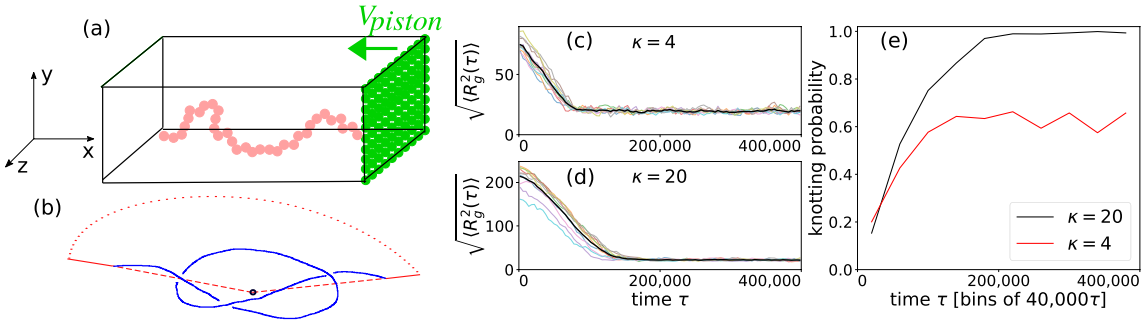


**Figure 3.** Schematics of the simulation model. (**a**) A semi-flexible bead-spring chain confined inside a rectangular nano-channel is pushed by the green piston from right to left at velocity $v = v_{\text{piston}}$. The confinement potentials are imposed on four (two *xy* and two *xz*) planes, and by the moving piston in the *yz* plane in the negative *x* direction. The chain is free to move on the side opposite the piston. This figure was created using Xfig (version 3.2.8a, URL: https://sourceforge.net/projects/mcj/). (**b**) Demonstration of the knot closure. The termini of the polymer are connected with the center of mass (black dot) as indicated by the dashed red lines. The solid red lines are then appended to the polymer and connected by a closing arc drawn with red dots. (**c**, **d**) The root-mean-squared radius of gyration $\sqrt{\langle R_g^2(\tau)\rangle}$ of the polymer as a function of LD time $\tau$ for 10 simulations each and two different values of the chain stiffness, $\kappa = 4$ and 20, respectively. The polymer is compressed until it reaches a steady state with a constant radius of gyration. At this point it moves like a blob of a fixed shape. The steady state $\sqrt{\langle R_g^2\rangle}$ for the polymer with lower stiffness is significantly smaller in its final state. (**e**) The knotting probability as a function of time $\tau$. During compression, the knotting probability increases while it is constant in the steady state. A higher stiffness leads to a higher knotting probability in the steady state. The results are averaged over 20 independent runs each.

## Methods

**Coarse-grained polymer model.** The coarse-grained polymer model for LD simulations used here is exactly the same as in our previous publication[47] where a bead-spring model polymer chain is confined to an open-ended rectangular channel and pushed from the right with a piston in the negative *x*-direction (Fig. 3a). The semi-flexible chain (Fig. 3b) is represented by a generalized bead-spring model[51] where the beads (monomers) interact via excluded volume (EV), a Finite Extension Nonlinear Elastic (FENE) spring potential and a bond-bending potential enabling variation of $\ell_p$ as implemented previously[46,47]. The excluded volume interaction between any two monomers *i* and *j* of diameter $\sigma$ is given by a short range truncated and shifted Lennard-Jones (LJ) potential $U_{\text{LJ}}$ (Eq. 1) of strength $\varepsilon$ with a cutoff distance $r_c = 2^{1/6}\sigma$ is given by:

$$\begin{aligned} U_{\text{LJ}} &= 4\varepsilon \sum_{i<j}^{N} \left[ \left(\frac{\sigma}{r_{ij}}\right)^{12} - \left(\frac{\sigma}{r_{ij}}\right)^{6} \right] + \varepsilon \quad \text{for } r_{ij} \le 2^{1/6}\sigma \\ &= 0 \qquad\qquad\qquad\qquad\quad \text{for } r_{ij} > 2^{1/6}\sigma, \end{aligned} \tag{1}$$

where $r_{ij} = |\vec{r}_i - \vec{r}_j|$ is the distance between any pair of beads. Successive monomers are connected by a FENE spring potential

$$U_{\text{FENE}} = -\frac{1}{2} k_{\text{FENE}} R_0^2 \sum_{i}^{N-1} \ln\left(1 - r_{i,i+1}^2/R_0^2\right), \tag{2}$$

where $k_{\text{FENE}}$ is the spring constant and $R_0$ is the maximum allowed bond length. The parameters $k_{\text{FENE}}$ and $R_0$ along with $\varepsilon$ and $\sigma$ determine the bond-length. The chain stiffness is controlled by a bond-bending potential

$$U_{\text{bend}} = \kappa \sum_{i=2}^{N-1} (1 - \cos\theta_i). \tag{3}$$

Here $\theta_i = \cos^{-1}\left(\frac{\vec{b}_{i-1}\cdot\vec{b}_i}{|\vec{b}_{i-1}||\vec{b}_i|}\right)$ is the angle between two successive bond vectors $\vec{b}_{i-1} = \vec{r}_i - \vec{r}_{i-1}$ and $\vec{b}_i = \vec{r}_{i+1} - \vec{r}_i$, respectively, as shown in Fig. 3b. In three dimensions, for $\kappa \neq 0$, the persistence length $\ell_p$ of the chain is related to $\kappa$ via[39,52,53]

$$\ell_p \approx \frac{\kappa\sigma}{k_B T}, \tag{4}$$

for the values of $\kappa$ considered in this work where $k_B$ is the Boltzmann constant and $T$ is the temperature.

**Langevin dynamics simulation.** We use the following Langevin dynamics equation of motion to advance the position of the *i*th monomer

$$m\ddot{\mathbf{r}}_i = -\nabla(U_{\mathrm{LJ}} + U_{\mathrm{FENE}} + U_{\mathrm{bend}} + U_{\mathrm{wall}} + U_{\mathrm{piston}}) + \gamma \mathbf{v}_i + \mathbf{W}_i, \tag{5}$$

where $\gamma$ is the monomer friction coefficient, and $\mathbf{W}_i$ is a Gaussian random force with zero mean at temperature $T$ which satisfies the fluctuation-dissipation relation. The numerical integration is implemented using the algorithm introduced by Gunsteren and Berendsen[54]. Our previous experience with LD simulations suggests that appropriate parameter specifications are $\gamma = 0.7\sqrt{m\varepsilon/\sigma^2}$, $k_{\mathrm{FENE}} = 30\varepsilon/\sigma$, $R_0 = 1.5\sigma$, and a temperature $k_BT/\varepsilon = 1.2$. For a time step $\Delta t = 0.01\tau$ (with $\tau$ being the standard Lennard-Jones time) these parameter values produce stable trajectories over a very long period of time and do not lead to an unphysical crossing of a bond by a monomer[55,56]. The average bond length stabilizes at $b_l = 0.970 \pm 0.002$ with negligible fluctuation regardless of chain size and rigidity[55]. The piston is moved with a constant velocity of $v_0 = 0.005\frac{\sigma}{\tau}$ if not noted otherwise after an initial equilibration of the chain. We ensure that the MD time for the pushing phase is long enough for the chain to attain a steady state shown in Fig. 3c–e that displays the connection between chain extension (Fig. 3c,d) and knot formation (Fig. 3e) in approach to the steady state. Times to reach the latter depend on bond stiffness $\kappa$ as seen from the behavior of $\langle\sqrt{\langle R_g^2(t)\rangle}\rangle$ in Fig. 3c,d. While for $\kappa = 4$ reaching a steady state takes less than $50{,}000\tau$, it takes around $160{,}000\tau$ for $\kappa = 20$. For each $\kappa$ and $v$, physical quantities are averaged over at least ten independent runs. Our analysis indicates that knots can form and dissolve both during the initial compression and in the steady state. Even compact structures can still change their knot type in accordance with other results on knot formation under applied force[38]. Of course, the probability of forming a knot, however, is significantly larger in the compressed (steady) state.

**Reptation Monte Carlo simulation to study the equilibrium limit.** Note that piston speeds in coarse-grained implicit solvent simulations are typically orders of magnitude faster when compared to experiments. Therefore, we have also undertaken reptation Monte Carlo simulations of a slightly simplified model system of a single semi-flexible bead-spring chain confined inside a rectangular nanochannel of fixed size. In the reptation move which resembles the movement of a slithering snake, one segment is deleted from a randomly chosen chain end and attached to the other end[57]. Moves are accepted based on the Metropolis criterion. The repulsive Lennard-Jones and bond-bending potentials were matched with those of the LD simulation as described above. However, contrary to the LD simulation model's confinement potential imposed onto the tube walls we use non-interacting walls and fixed bond length $b_l = 0.967$. These MC simulations allow for a comparison of our dynamical investigations with equilibrium values (corresponding to piston velocity $v \to 0$).

**Knot analysis.** Knots in a closed chain are typically characterized by the minimum number of crossings observed when projecting a 3D chain onto a plane and can be considered as a fine gauge for the overall structure. Apart from the unknotted ring, the so-called unknot, the simplest knot is the trefoil ($3_1$) knot, which contains three crossings. There is one knot type with four crossings ($4_1$) and two with five crossings, and from there on the number of different knots with the same number of crossings increases exponentially[58,59]. In our setup the polymer chain is open, and therefore, a closure connecting both ends of the chain has to be defined. First, we connect the end-points of each polymer with its center of mass. Along these lines we define a closure which emerges from one terminus follows the first line connects to the second one far away from the polymer and ends at the second terminus[40]. After closure, the Alexander polynomial can be determined as described in detail in[60] (compare Fig. 3b). Knot sizes are determined by successively removing monomers from the ends of a polymer until the knot type changes[29].

**Mapping onto DNA and comparison with experiments.** Mapping our semi-flexible chain onto DNA is based on Eq. (4). For simplicity, we assume a solvent-independent persistence length of 50 nm or 150 base pairs. Furthermore, we assume that our beads describe the locus of a double-stranded DNA strand. In high salt conditions (1M NaCl), charges of DNA are completely screened and $\sigma \approx 2.5$ nm. In physiological conditions charges are only partially screened and $\sigma \approx 5$ nm, and for low salt conditions $\sigma$ increases even further to about 15 nm at 0.01 M NaCl[33,39,61]. With a simulation temperature of $T = 1.2$ used throughout we obtain (in simulation units) $\kappa = 24$ for high salt, $\kappa = 12$ for physiological and $\kappa = 4$ for low salt conditions. This allows us to put our simulations in the context of recent experiments by Amin et al.[16] undertaken at an estimated ionic strength of 8 $mM$ which corresponds to our low salt scenario. Our chain has a contour length of $L = N\sigma = 1024\sigma = 15{,}360$ nm or 46,080 base pairs, while our confining tube has a width of $16\sigma \approx 240$ nm. This compares to 168,903 base pairs and tube dimensions of $325 \times 415$ nm used in Ref.[16]. Note that the mapping changes drastically with ionic conditions.

The time scale of the simulated quantities can be translated into an experimental time scale via

$$t_{MD} = \sigma\sqrt{\frac{m}{k_BT}}. \tag{6}$$

For low salt conditions we use $\sigma = 15$ nm as stated above, a mass $m$ of 618u per base pair, a persistence length of $\frac{\kappa\sigma}{k_BT} = 3.33$ beads and therefore 45 base pairs per bead. We assume room temperature of $T = 300$. This results in a time scale of 1 simulation time which equals to approximately 1.6ns. Our simulation time of $400{,}000\tau$ for $\kappa = 4$ is therefore equivalent to $6.4 \times 10^{-4}$ s. Hence without explicit solvent one obtains a much faster time scale compared to experiments which often take place at a scale of seconds[16]. A typical experimental piston velocity for these experiments is 0.1–1 μm/s[14,15]. In the simulation we advance the piston with a velocity $v_0 = 0.005\frac{\sigma}{\tau} \approx 0.05$ m/s, several order of magnitude faster than the experimental piston speed. Thus dynamics in our coarse-grained

simulation are accelerated by several orders of magnitude in comparison to experiments and cannot be compared directly.

Received: 13 December 2021; Accepted: 17 March 2022
Published online: 29 March 2022

## References

1. Marenduzzo, D., Micheletti, C. & Orlandini, E. Biopolymer organization upon confinement. *J. Phys. Condens. Matt.* **22**, 283102 (2010).
2. Reisner, W., Pedersen, J. N. & Austin, R. H. DNA confinement in nanochannels: Physics and biological applications. *Rep. Prog. Phys.* **75**, 106601 (2012).
3. Arsuaga, J., Vazquez, M., Trigueros, S., Sumners, D. W. & Roca, J. Knotting probability of DNA molecules confined in restricted volumes: DNA knotting in phage capsids. *PNAS* **99**, 5373–5377 (2002).
4. Arsuaga, J. *et al.* DNA knots reveal a chiral organization of DNA in phage capsids. *PNAS* **102**, 9165–9169 (2005).
5. Petrov, A. S. & Harvey, S. C. Packaging double-helical DNA into viral capsids: Structures, forces, and energetics. *Biophys. J.* **95**, 497 (2008).
6. Marenduzzo, D. *et al.* DNA–DNA interactions in bacteriophage capsids are responsible for the observed DNA knotting. *PNAS* **106**, 22269–22274 (2009).
7. Reith, D., Cifra, P., Stasiak, A. & Virnau, P. Effective stiffening of DNA due to nematic ordering causes DNA molecules packed in phage capsids to preferentially form torus knots. *Nucleic Acids Res.* **40**, 5129–5137 (2012).
8. Marenduzzo, D., Micheletti, C., Orlandini, E. & Sumners, D. W. Topological friction strongly affects viral DNA ejection. *PNAS* **110**, 20081–20086 (2013).
9. Berndsen, Z. T., Keller, N., Grimes, S., Jardine, P. J. & Smith, D. E. Nonequilibrium dynamics and ultraslow relaxation of confined DNA during viral packaging. *PNAS* **111**, 8345 (2014).
10. Keller, N., Grimes, S., Jardine, P. J. & Smith, D. E. Single DNA molecule jamming and history-dependent dynamics during motor-driven viral packaging. *Nat. Phys.* **12**, 757 (2016).
11. Kim, Y. *et al.* Nanochannel confinement: DNA stretch approaching full contour length. *Lab Chip* **11**, 1721 (2011).
12. Stein, D., van der Heyden, H. J., Koopmas, W. J. A. & Dekker, C. Pressure-driven transport of confined DNA polymers in fluidic channels. *PNAS* **3**, 15853 (2006).
13. Mikkelsen, M. B., Reisner, W., Flyvbjerg, H. & Kristensen, A. Pressure-driven DNA in nanogroove arrays: Complex dynamics leads to length- and topology-dependent separation. *Nano Lett.* **11**, 1598 (2011).
14. Khorshid, A. *et al.* Dynamic compression of single nanochannel confined DNA via a nanodozer assay. *Phys. Rev. Lett.* **113**, 268104 (2014).
15. Khorshid, A., Amin, S., Zhang, Z., Sakaue, T. & Reisner, W. Non-equilibrium dynamics of nanochannel confined dna. *Macromolecules* **49**, 1933 (2016).
16. Amin, S., Khorshid, A., Zeng, L., Zimny, P. & Reisner, W. A nanofluidic knot factory based on compression of single DNA in nanochannels. *Nat. Commun.* **9**, 1506–1506 (2018).
17. Lam, T. E. *et al.* Genome mapping on nanochannel arrays for structural variation analysis and sequence assembly. *Nat. Biotechnol.* **30**, 771 (2012).
18. Zhou, J. *et al.* Enhanced nanochannel translocation and localization of genomic DNA molecules using three-dimensional nanofunnels. *Nat. Commun.* **8**, 807 (2017).
19. Plesa, C. *et al.* Direct observation of DNA knots using a solid-state nanopore. *Nat. Nanotechnol.* **11**, 1093–1097 (2016).
20. Suma, A. & Micheletti, C. Pore translocation of knotted DNA rings. *Proc. Natl. Acad. Sci.* **114**, E2991–E2997 (2017).
21. Sakaue, T. Semiflexible polymer confined in closed spaces. *Macromolecules* **40**, 5206 (2007).
22. Jun, S., Thirumalai, D. & Ha, B.-Y. Compression and stretching of a self-avoiding chain in cylindrical nanopores. *Phys. Rev. Lett.* **101**, 138101 (2008).
23. Micheletti, C., Marenduzzo, D. & Orlandini, E. Polymers with spatial or topological constraints: Theoretical and computational results. *Phys. Rep.* **504**, 1–73 (2011).
24. Vologodskii, A. V., Lukashin, A. V. & Frank-Kamenetskii, M. D. Topological interaction between polymer chains. *Sov. Phys. JETP* **40**, 932–936 (1974).
25. Koniaris, K. & Muthukumar, M. Knottedness in ring polymers. *Phys. Rev. Lett.* **66**, 2211–2214 (1991).
26. Mansfield, M. L. Knots in Hamilton cycles. *Macromolecules* **27**, 5924–5926 (1994).
27. Grosberg, A. Y. Critical exponents for random knots. *Phys. Rev. Lett.* **85**, 3858–3861 (2000).
28. Marcone, B., Orlandini, E., Stella, A. L. & Zonta, F. What is the length of a knot in a polymer?. *J. Phys. Math. Gen.* **38**, L15–L21 (2005).
29. Virnau, P., Kantor, Y. & Kardar, M. Knots in globule and coil phases of a model polyethylene. *JACS* **127**, 15102 (2005).
30. Foteinopoulou, K., Karayiannis, N. C., Laso, M., Kröger, M. & Mansfield, M. L. Universal scaling, entanglements, and knots of model chain molecules. *Phys. Rev. Lett.* **101**, 265702 (2008).
31. Orlandini, E. & Micheletti, C. Knotting of linear DNA in nano-slits and nano-channels: A numerical study. *J. Biol. Phys.* **39**, 267–275 (2013).
32. Micheletti, C. & Orlandini, E. Knotting and unknotting dynamics of DNA strands in nanochannels. *ACS Macro Lett.* **3**, 876–880 (2014).
33. Trefz, B., Siebert, J. & Virnau, P. How molecular knots can pass through each other. *PNAS* **111**, 7948 (2014).
34. Coronel, L., Orlandini, E. & Micheletti, C. Non-monotonic knotting probability and knot length of semiflexible rings: The competing roles of entropy and bending energy. *Soft Matter* **13**, 4260 (2017).
35. Meyer, H., Horwath, E. & Virnau, P. Mapping onto ideal chains overestimates self-entanglements in polymer melts. *ACS Macro Lett.* **7**, 757–761 (2018).
36. Zhang, J., Meyer, H., Virnau, P. & Daoulas, K. C. Can soft models describe polymer knots?. *Macromolecules* **53**, 10475–10486 (2020).
37. Tubiana, L. *et al.* Comparing equilibration schemes of high-molecular-weight polymer melts with topological indicators. *J. Phys. Condens. Matter.* **33**, 204003 (2021).
38. Michieletto, D., Orlandini, E., Turner, M. S. & Micheletti, C. Separation of geometrical and topological entanglement in confined polymers driven out of equilibrium. *ACS Macro Lett.* **9**, 1081–1085 (2020).
39. Rieger, F. C. & Virnau, P. A Monte Carlo study of knots in long double-stranded DNA chains. *PLoS Comput. Biol* **12**, e1005029 (2016).
40. Virnau, P., Mirny, L. & Kardar, M. Intricate knots in proteins: Function and evolution. *PLoS Comput. Biol.* **2**, e122 (2006).
41. Sulkowska, J. I., Sulkowski, P., Szymczak, P. & Cieplak, M. Stabilizing effect of knots on proteins. *PNAS* **105**, 19714–19719 (2008).
42. Sulkowska, J. I., Sulkowski, P. & Onuchic, J. Dodging the crisis of folding proteins with knots. *PNAS* **106**, 3119–3124 (2009).
43. Boelinger, D. *et al.* A stevedore's protein knot. *PLoS Comput. Biol.* **6**, e1000731 (2010).

44. Jamroz, M. *et al.* Knotprot: A database of proteins with knots and slipknots. *Nucleic Acids Res.* **43**, D306–D314 (2015).
45. Wüst, T., Reith, D. & Virnau, P. Sequence determines degree of knottedness in a coarse-grained protein model. *Phys. Rev. Lett.* **114**, 028102 (2015).
46. Huang, A., Reisner, W. & Bhattacharya, A. Dynamics of DNA squeezed inside a nanochannel via a sliding gasket. *Polymers* **8**, 352 (2016).
47. Bernier, S., Huang, A., Reisner, W. & Bhattacharya, A. Evolution of nested folding states in compression of a strongly confined semiflexible chain. *Macromoecules* **51**, 4012 (2018).
48. Hayase, Y., Sakaue, T. & Nakanishi, H. Compressive response and helix formation of a semiflexible polymer confined in a nanochannel. *Phys. Rev. E.* **95**, 052502 (2017).
49. Humphrey, W., Dalke, A. & Schulten, K. VMD—Visual molecular dynamics. *J. Mol. Graph* **14**, 33 (1996).
50. Dorfman, K. D., Gupta, D., Jain, A., Muralidhar, A. & Tree, D. R. Hydrodynamics of DNA confined in nanoslits and nanochannels. *Eur. Phys. J. Spec. Top.* **223**, 3179–3200 (2014).
51. Grest, G. S. & Kremer, K. Molecular dynamics simulation for polymers in the presence of a heat bath. *Phys. Rev. A* **33**, 3628–3631 (1986).
52. Hsu, H.-P. & Binder, K. Stretching semiflexible polymer chains: Evidence for the importance of excluded volume effects from Monte Carlo simulation. *J. Chem. Phys.* **136**, 024901 (2012).
53. Fixman, M. & Kovac, J. Polymer conformational statistics. III. Modified Gaussian models of stiff chains. *J. Chem. Phys.* **58**, 1564–1568 (1973).
54. van Gunsteren, W. F. & Berendsen, H. J. C. Algorithms for Brownian dynamics. *Mol. Phys.* **45**, 637 (1982).
55. Huang, A., Bhattacharya, A. & Binder, K. Conformations, transverse fluctuations, and crossover dynamics of a semi-flexible chain in two dimensions. *J. Chem. Phys.* **140**, 214902 (2014).
56. Huang, A., Hsu, H.-P., Bhattacharya, A. & Binder, K. Semiflexible macromolecules in quasi-one-dimensional confinement: Discrete versus continuous bond angles. *J. Chem. Phys.* **143**, 243102 (2015).
57. Wall, F. T. & Mandel, F. Macromolecular dimensions obtained by an efficient Monte Carlo method without sample attrition. *J. Chem. Phys.* **63**, 4592–4595 (1975).
58. Rolfsen, D. *Knots and Links. Mathematics Lecture Series* (Publish or Perish, 1976).
59. Adams, C. *The Knot Book* (W.H. Freeman, 1994).
60. Virnau, P. Detection and visualization of physical knots in macromolecules. *Phys. Proc.* **6**, 114 (2010).
61. Rybenkov, V. V., Cozzarelli, N. R. & Vologodskii, A. V. Probability of DNA knotting and the effective diameter of the DNA double helix. *PNAS* **90**, 5307–5311 (1993).


## Acknowledgements

The authors acknowledge partial funding from TopDyn. We are grateful to the Deutsche Forschungsgemeinschaft (DFG, German Research Foundation) for funding this research: Project Number 233630050-TRR 146. The LD simulation were carried out at the UCF's high performance computing cluster STOKES. The authors gratefully acknowledge the computing time granted on the supercomputer Mogon offered by the Johannes Gutenberg University Mainz (hpc.uni-mainz.de), which is a member of the AHRP (Alliance for High Performance Computing in Rhineland Palatinate, http://www.ahrp.info) and the Gauss Alliance e.V.. A.B. acknowledges travel support from Institut für Physik, Mainz. A.B. thanks Aiqun Huang for the preliminary runs.

## Author contributions

A.B. performed the LD simulations. S.W. performed the Monte Carlo simulations. J.R and P.V. analyzed the results. All authors reviewed the manuscript.

## Funding

Open Access funding enabled and organized by Projekt DEAL.

## Competing interests

The authors declare no competing interests.

## Additional information

**Correspondence** and requests for materials should be addressed to P.V. or A.B.

**Reprints and permissions information** is available at www.nature.com/reprints.

**Publisher's note** Springer Nature remains neutral with regard to jurisdictional claims in published maps and institutional affiliations.